Supporting Information

Deciphering the role of anionic group in zwitterionic electron transport layers for organic solar cells

Longhai Pan†, Feng Han†, Nade Chen†, Wentian Han, Huixiang Zhang, Huayi Liu, Wenxu Liu* and Yao Liu*

State Key Laboratory of Chemical Resource Engineering, Beijing Advanced Innovation Center for Soft Matter Science and Engineering, College of Chemistry, Beijing University of Chemical Technology, Beijing, 100029, China.

E-mail: liuwenxu@buct.edu.cn; liuyao@mail.buct.edu.cn

1. Experimental section

1.1 Materials and measurements

Materials: All the chemicals utilized in this study were purchased from commercial suppliers and were employed directly without additional purification procedures. PM6 and Y6 were purchased form Solarmer Materials. D18 was received from hyperchemical. L8-BO and BTP-eC9 were purchased from eFlexPV Limited (China). PFN-Br was obtained from Derthon Optoelectronics Materials Science Technology Co. LTD. Poly(3,4-ethylene-dioxythiophene):poly(styrenesulfonate) (PEDOT:PSS) was purchased from Heraeus.

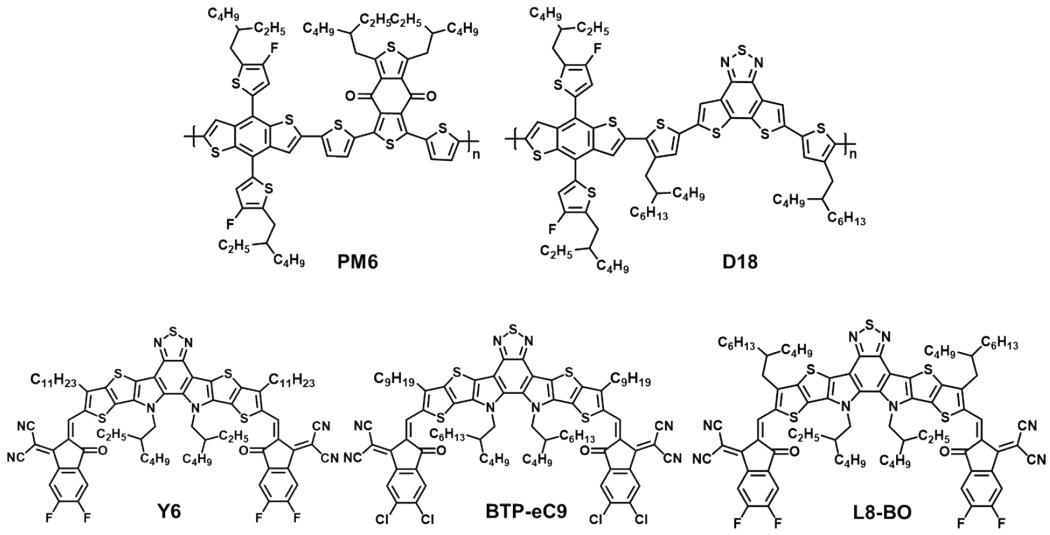

Scheme S1. Chemical structures of the polymer donors and FREAs used in this study.

Measurements: Nuclear magnetic resonance (NMR) spectra were acquired using Bruker Avance III instrument with CF_3COOD (TFA-*d*) or $(CD_3)_2SO$ (DMSO-d_6) as the solvents. Mass spectra (MALDI-TOF MS) were conducted on a Bruker BIFLEX III mass spectrometer. Thermal stability analysis was carried out on a HITACHI STA7300 analyzer under N_2 atmosphere, with a heating rate of 10 °C min^{-1} up to 500 °C. Ultraviolet photoelectron spectroscopy (UPS) measurements were conducted with a

Thermo Escalab XI+ instrument that was furnished with a helium discharge lamp emitting (He I line, 21.2 eV) as the ultraviolet excitation source, along with a hemispherical SPHERA energy analyzer. During UPS measurement, −6 eV bias was applied to all samples to compensate for the instrument work-function difference that repels low-kinetic energy electron. SKP measurements were performed using a KP Technology Model SKP 5050. Transient photocurrent (TPC) and transient photovoltage (TPV) were recorded on the Setfos-Paiso Integration (SPI) Module V 3.0 test system. Atomic force microscopy (AFM) images were obtained on a Bruker microscope in tapping mode. Cyclic voltammetry (CV) curves were recorded on a CHI 660e electrochemical analyzer with tetrabutylammonium phosphorus hexafluoride (Bu_4NPF_6, 0.1 M in acetonitrile) as the supporting electrolyte at a scan rate of 100 mV s^{-1}. A glass carbon disk, a Pt wire, and a saturated Ag/AgCl electrode were respectively selected as the working electrode, counter electrode and reference electrode. The samples were prepared by drop-cast the TFE solutions on the polished working electrodes. The ferrocene/ferrocenium (Fc/Fc^+) redox couple was used to calibrate the potential before tests, and the $\varphi_{Fc+/Fc}$ was estimated to be 0.40 V. For GIWAXS measurements, an X-ray beam with a wavelength of 1.240 Å was directed at the sample at grazing angles that were both above and below the critical angle of the polymer film ($\alpha_c = 0.16$) yet remained below the critical angle of the silicon substrate ($\alpha_c = 0.22$), and the scattered intensity was detected using a PILATUS 1M detector.

1.2 Device fabrication and characterization

OSCs were fabricated using normal construction of ITO/PEDOT:PSS/active layer/ETL/Ag. First, the ITO glass substrates were sequentially cleaned with commercial detergent, deionized water, acetone, and isopropyl alcohol. Subsequently, the substrate was treated with ultraviolet ozone (UVO) for 15 minutes. The aqueous solution of PEDOT:PSS was spin-coated on ITO substrates at 3500 rpm for 40 s and then annealed at 150 °C for 15 min under ambient conditions. Afterwards, it was placed in a glove box (nitrogen atmosphere, O_2 < 1 ppm, H_2O < 1 ppm). The active layers (PM6:Y6, PM6:BTP-eC9, PM6:L8-BO) were sequentially prepared using the following procedures: (1) PM6:Y6 (1:1.2, w:w, 14 mg mL^{-1} in total) was dissolved in chloroform with 0.5 vol% 1-chloronaphthalene and the solution was spin-coated at 1500 rpm for 40 s, which was allowed to thermally annealing at 80 °C for 10 min. (2) PM6:BTP-eC9 (1:1.2, w/w, 15.4 mg mL^{-1} in total) was dissolved in chloroform with 10 mg mL^{-1} 1,3,5-trichlorobenzene (TCB) and spin-cast onto the HTL at 2500 rpm for 30 s, followed by thermal annealing at 100 ℃ for 5 min. (3) PM6:L8-BO (1:1.2, w/w, 15.4 mg mL^{-1} in total) was dissolved in chloroform with 0.25 vol% diiodomethane (DIM) as additive, then spin-deposited at 2000 rpm for 40 s and thermally annealed at 90 ℃ for 10 min. (4) D18:L8-BO (1:1, w/w, 14 mg mL^{-1} in total) was dissolved in chloroform with 0.25 vol% DIM as additive, then spin-deposited at 3000 rpm for 40 s and thermally annealed at 90 ℃ for 10 min.

Following this, TFE solutions of ETLs at varying concentrations were spin-coated onto the active layer, resulting in ETLs of differing thicknesses. The substrate was then transferred to a thermal evaporation system for depositing a 100 nm-thick Ag cathode

under a high vacuum of 1×10^{-6} mbar. *J–V* characteristics were measured in a nitrogen-filled glovebox using a Keithley 2400), under AM 1.5 G simulated solar illumination provided by a 300 W xenon (Xe) solar simulator (SS-F5-3A, ENLITECH). The incident light intensity was calibrated with a reference silicon solar cell. External quantum efficiency (EQE) measurements were conducted with a calibrated QE-R3011 quantum efficiency tester (ENLITECH), utilizing a Xe lamp as the excitation source.

1.3 Conductivity measurements

The solution of zwitterions was spin-coated onto glass substrates. Then, Ag with thickness of 100 nm was deposited on the ETLs as electrode. The conductivity was measured using a Keithley 4200 SCS-equipped probe station in a N_2-filled glove box. The conductivity was calculated using the formula of

$$\sigma = \frac{I \times L}{V \times W \times T}$$

Where σ corresponds to the conductivity; I represents the measured current; V is applied voltage; W refers to the length of the Ag electrode (1300 μm); L signifies the electrode separation distance (50 μm); and T indicated the thickness of organic layer (40 nm).

1.4 Electron mobility measurements

The fabrication of electron-only devices with structure of ITO/ETLs/Al was analogous to that of the previously described OSCs. Electron mobilities (μ_es) were calculated by the Mott Gurney equation

$$J = \frac{9}{8}\varepsilon_0\varepsilon_r\mu_e\frac{V^2}{L^3}$$

Here, V is applied voltage; μ_e represents the electron mobility; ε_0 and ε_r respectively denote the vacuum permittivity and relative permittivity; J represents the

current density and L is the thickness of the film.

2. Synthetic Section

2.1. Materials

Unless otherwise noted, all the chemicals were obtained from commercial sources and used as received. Anhydrous solvents were distilled by standard procedures prior to use. PDI-M and 2-(1,3-dioxolan-2-ylidene)malononitrile were synthesized according to the reported literature.[1,2]

2.2. Synthetic details and characterizations

PDIM-DC: PDI-M (0.2 g, 0.33 mmol) and 2-(1,3-dioxolan-2-ylidene)malononitrile (0.14 g, 1 mmol) was dissolved in trifluoroethanol (20 mL). The reaction was heated at 60 °C for 2 days. After cooling down to room temperature, the solvent was removed under reduced pressure and the resulting residue was poured into acetone (30 mL). The precipitation was collected and dried under vacuum to yield PDIM-DC as a red solid (0.26 g, 90%).^{1}H NMR (400 MHz, DMSO-d_6), δ (ppm): 9.16 (s, 2H), 8.00–7.71 (m, 12H), 4.52–4.41 (m, 4H), 4.40–4.30 (m, 4H), 4.30–4.23 (m, 4H), 4.09–4.01 (m, 4H), 2.35–2.22 (m, 4H). ^{13}C NMR (101 MHz, TFA-*d*), δ (ppm): 165.54, 136.29, 135.78, 132.78, 129.14, 126.03, 124.27, 123.56, 123.46, 123.03, 122.13, 121.88, 63.92, 62.97, 49.00, 48.08, 37.91, 28.33. ESI (m/z): calculated for $C_{48}H_{34}N_{10}O_8$: 878.86, found: 879.26 $[M+H]^+$.

PDIM-z: The synthetic procedure of PDIM-z was similar to that of PDIM-DC except that Compound 1 was replaced by 1,3-propanesultone. PDIM-z was obtained as a red solid (0.22 g, 80%). ^{1}H NMR (400 MHz, TFA-*d*), δ (ppm): 9.06 (s, 2H), 9.00 (s,

8H) 7.76 (s, 2H), 7.70 (s, 2H), 4.76–4.69 (t, J = 7.4 Hz, 4H), 4.69–4.62 (t, J = 6.2 Hz, 4H), 4.09–3.06 (m, 4H), 3.55–3.47 (m, 4H), 2.81–2.70 (m, 4H), 2.48–2.40 (m, 4H). ^{13}C NMR (101 MHz, TFA-*d*), δ (ppm): 165.64, 136.24, 135.83, 132.97, 129.23, 126.14, 124.37, 122.97, 122.12, 121.98, 48.33, 47.97, 47.81, 37.97, 28.25, 24.91. ESI (m/z): calculated for $C_{42}H_{38}N_6O_{10}S_2$: 850.21, found: 851.23 $[M+H]^+$.

3. Thermal stability and optoelectronic properties characterizations of the ETLs.

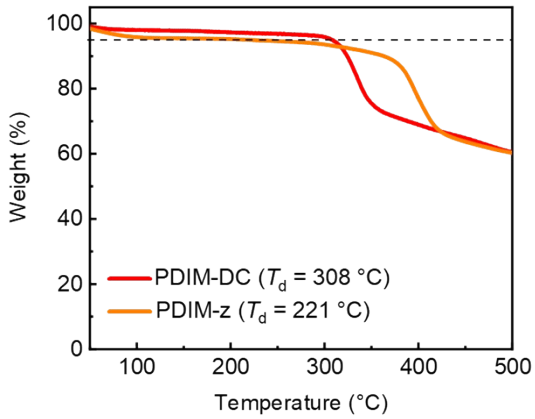

Figure S1. TGA curves of PDIM-DC and PDIM-z under N_2 atmosphere with a heating rate of 10 °C min^{-1}.

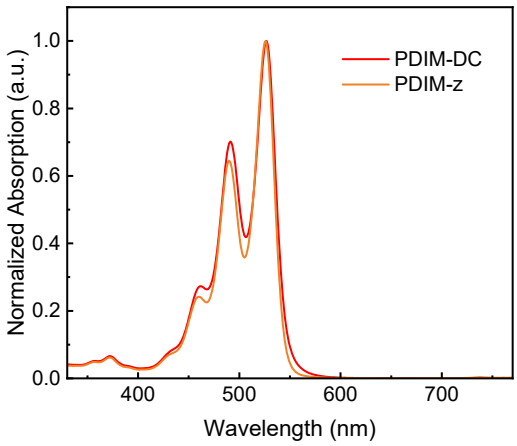

Figure S2. Absorption spectra of the zwitterions in dilute TFE solution.

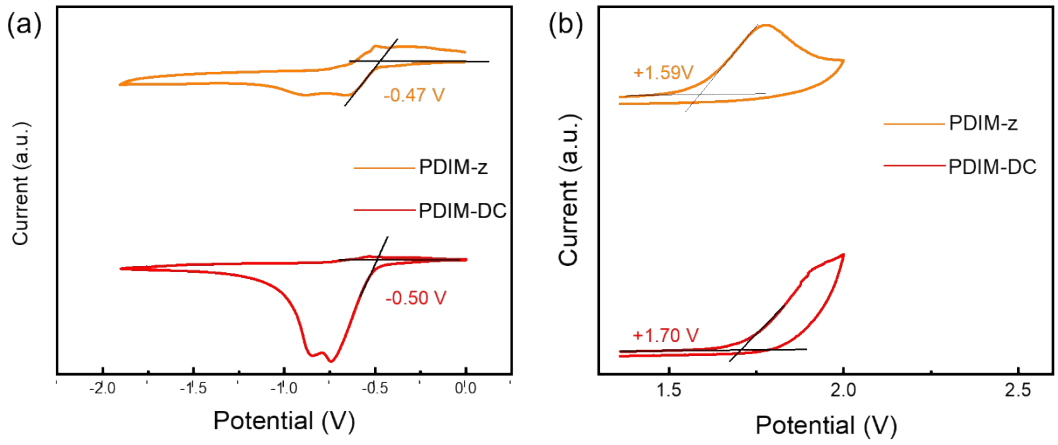

Figure S3. Cyclic voltammogram curves of PDIM-DC and PDIM-z.

According to the equation of $E_{HOMO/LUMO} = -e(\varphi_{ox/red} + 4.8 - \varphi_{Fc/Fc+})$, the frontier energy levels of the zwitterions are calculated as follow:

For PDIM-DC: $E_{HOMO} = -e(1.70 + 4.8 - 0.40) = -6.10$ eV;

$E_{LUMO} = -e(-0.50 + 4.8 - 0.40) = -3.90$ eV;

For PDIM-z: $E_{HOMO} = -e(1.59 + 4.8 - 0.40) = -5.99$ eV;

$E_{LUMO} = -e(-0.47 + 4.8 - 0.40) = -3.93$ eV.

Table S1. Optoelectronic properties of PDIM-DC and PDIM-z.

ETLs	$\lambda_{max, sol}$ [a] (nm)	$\lambda_{max, film}$ [a] (nm)	λ_{edge} [a] (nm)	E_g^{opt} [a] (eV)	E_{HOMO} [b] (eV)	E_{LUMO} [b] (eV)	E_{HOMO} [c] (eV)
PDIM-DC	526	501	625	1.98	–6.10	–3.90	–6.09
PDIM-z	526	481	610	2.03	–5.99	–3.93	–5.99

[a]The data are derived from UV-vis absorption spectra, where $E_g^{opt} = 1240/\lambda_{edge}$, with λ_{edge} referring to the absorption onset; [b]The $E_{HOMO/LUMO}$ are determined via CV measurements using the formula: $E_{HOMO/LUMO} = -e\ (4.8 + \varphi_{ox/red} - \varphi_{Fc/Fc+})$ (eV), where the value of $\varphi_{Fc/Fc+}$ is 0.40 eV; [c]The E_{HOMO} is calculated by the formula: $E_{HOMO} = E_{LUMO} - E_g^{opt}$; [d]The E_{HOMO} is calculated based on UPS data.

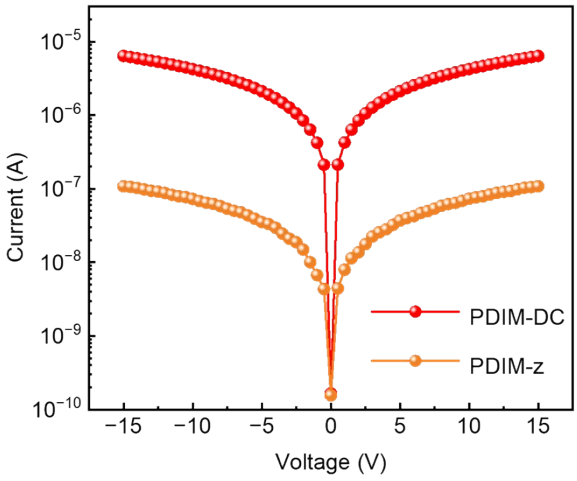

Figure S4. Electrical conductivity of PDIM-DC and PDIM-z.

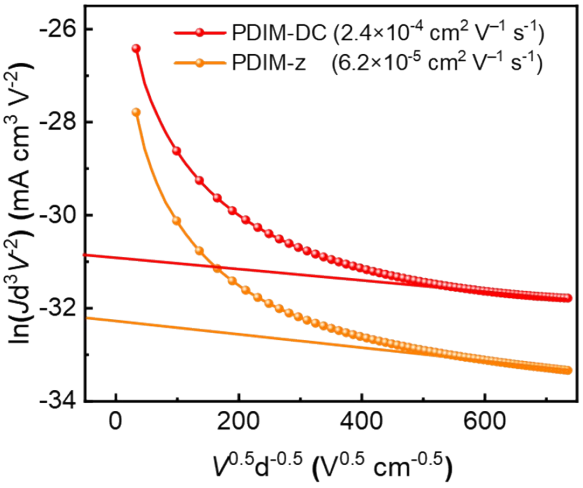

Figure S5. For electron-only devices with the configuration of ITO/ETLs/Al.

Table S2. A summary of the electrical properties of PDIM-DC and PDIM-z.

ETLs	Conductivity (S cm^{-1})	Mobility (cm^2 V^{-1} s^{-1})
PDIM-DC	2.12×10^{-3}	2.4×10^{-4}
PDIM-z	3.66×10^{-5}	6.2×10^{-5}

4. Device fabrication and photovoltaic performances characterizations

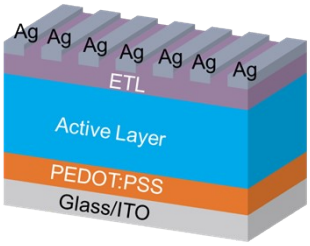

Figure S6. Device configuration of the conventional OSCs in this work.

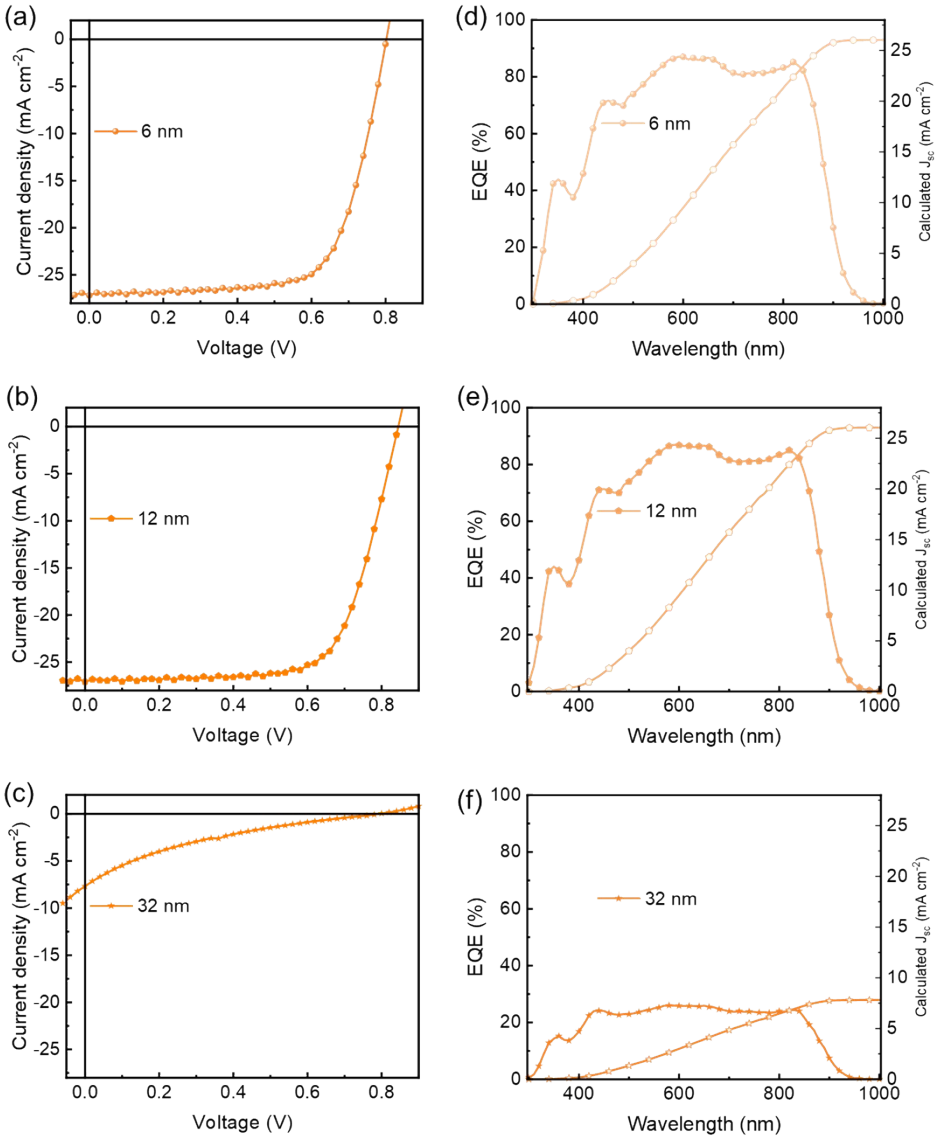

Figure S7. (a-c) *J–V* and (d-f) EQE curves of optimal devices based on the PM6:Y6 system with varying thicknesses of PDIM-z as ETLs.

Table S3. A summary of device parameters based on the PM6:Y6 system with varying thicknesses of PDIM-z as ETLs.

Thickness (nm)	V_{oc} [a] (V)	J_{sc} [a] (mA cm^{-2})	FF [a] (%)	PCE[a] (%)
6	0.802 (0.799±0.006)	26.99 [26.03] (26.81±0.15)	69.12 (68.67±0.55)	14.96 (14.69±0.23)
12	0.845 (0.844±0.002)	26.88 [26.05] (26.70±0.18)	68.91 (68.18±1.07)	15.65 (15.36±0.18)
32	0.793 (0.757±0.033)	7.68 [7.81] (6.01±0.97)	14.92 (17.85±2.35)	0.909 (0.80±0.06)

[a]Average value from at least 10 devices.

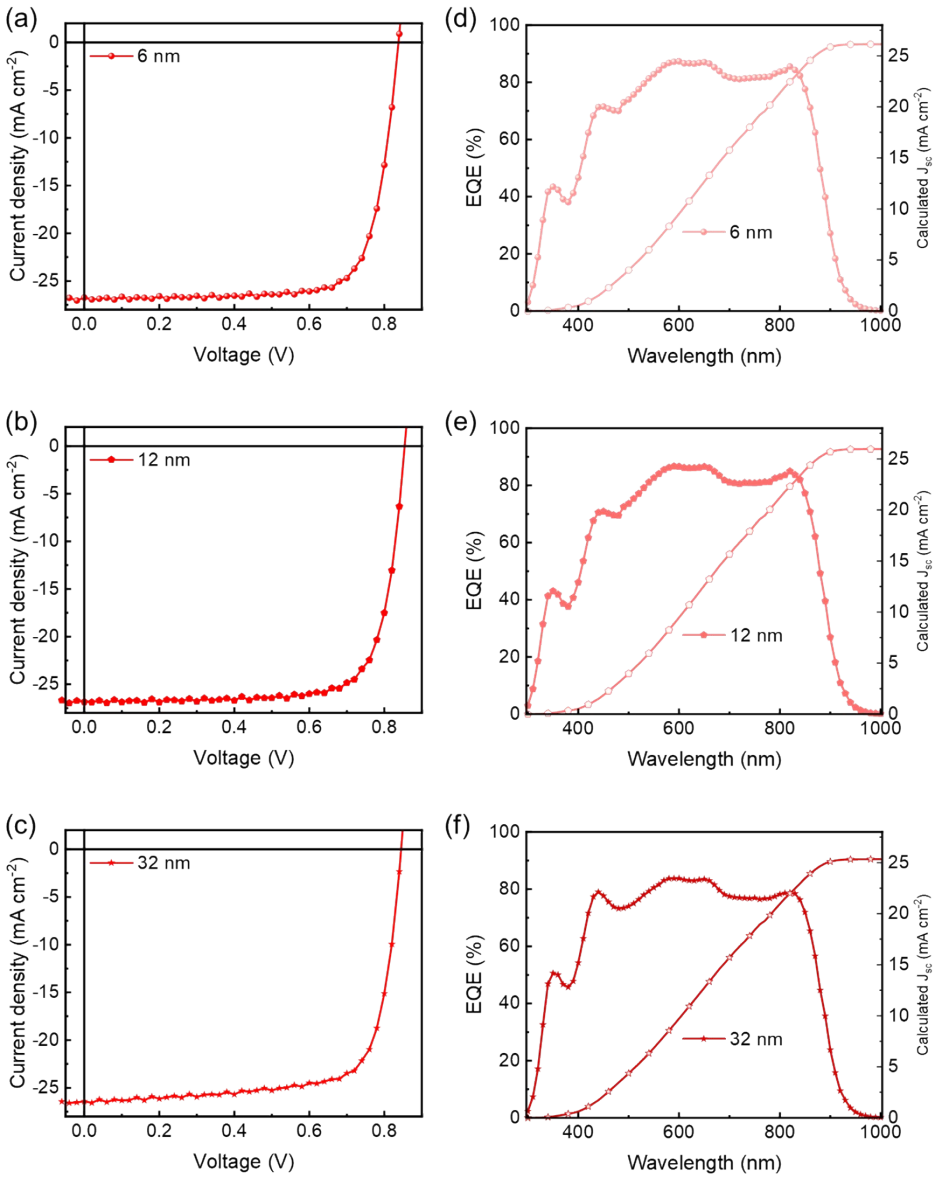

Figure S8. (a-c) *J–V* and (d-f) EQE curves of optimal devices based on the PM6:Y6 system with varying thicknesses of PDIM-DC as ETLs.

Table S4. A summary of device parameters based on the PM6:Y6 system with varying thicknesses of PDIM-DC as ETLs.

Thickness (nm)	V_{oc} [a] (V)	J_{sc} [a] (mA cm^{-2})	FF [a] (%)	PCE[a] (%)
6	0.836 (0.833±0.002)	26.90 [26.14] (26.85±0.08)	76.16 (76.13±0.38)	17.13 (17.02±0.08)
12	0.854 (0.852±0.002)	26.84 [25.97] (26.75±0.14)	76.92 (76.87±0.36)	17.64 (17.51±0.09)
32	0.843 (0.843±0.002)	26.50 [25.33] (26.57±0.19)	73.93 (73.23±0.77)	16.52 (16.40±0.10)

[a]Average value from at least 10 devices.

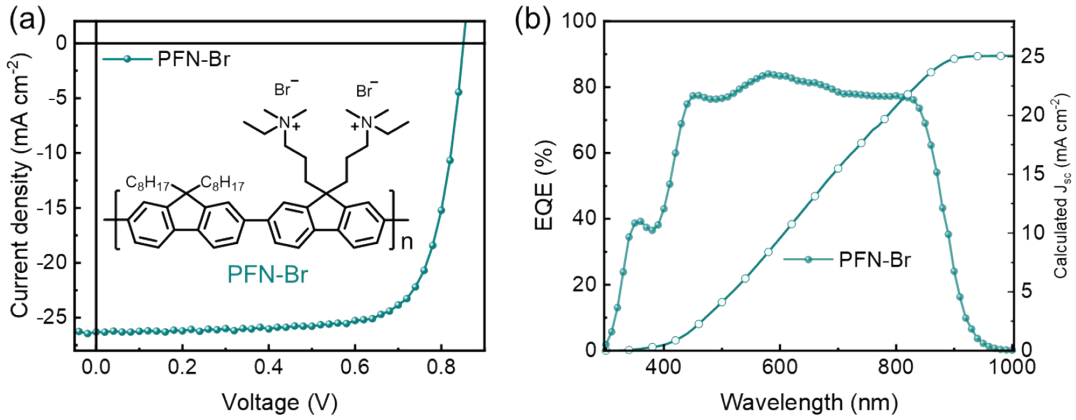

Figure S9. (a) *J*–*V* curve (Inset: Chemical structure of PFN-Br) and (b) EQE spectrum of the optimal device containing PFN-Br interlayer and PM6:Y6 active layer.

Table S5. A summary of device parameters based on the PM6:Y6 system with PFN-Br as ETL.

Thickness (nm)	V_{oc} [a] (V)	J_{sc} [a] (mA cm^{-2})	FF [a] (%)	PCE[a] (%)
5	0.850 (0.849±0.009)	26.35 [25.06] (26.18±0.20)	74.51 (74.54±0.68)	16.68 (16.54±0.28)

[a]Average value from at least 10 devices.

Table S6. The P_{diss} and P_{coll} values of the OSCs with and without ETLs.

ETLs	P_{diss}[a]	P_{coll}[b]
Bare-Ag	96.5%	74.0%
PDIM-DC	98.4%	90.2%
PDIM-z	97.4%	89.5%

[a]The exciton dissociation probability; [b]The charge collection probability.

To evaluate the effects of PDIM-DC and PDIM-z as ETLs on the exciton dissociation (P_{diss}) and charge collection (P_{coll}) characteristics of the devices through the relationship between the photocurrent density (J_{ph}) and its effective voltage (V_{eff}). J_{ph} are defined by the $J_{ph}=J_L - J_D$ (J_L stands for the current density during illumination, and J_D indicates the current density in darkness). The effective voltage (V_{eff}) is defined as $V_0 - V_{app}$, where V_0 denotes the voltage at which J_{ph} equals zero and V_{app} is the externally applied voltage. At sufficiently high V_{eff}, all excitons are dissociated into free charge carriers, which are fully collected by the electrodes, resulting in the saturation of $J_{ph,sat}$. The $J_{ph}/J_{ph,sat}$ ratio was computed to evaluate P_{diss} under short-circuit conditions and P_{coll} at the maximum power point, respectively.

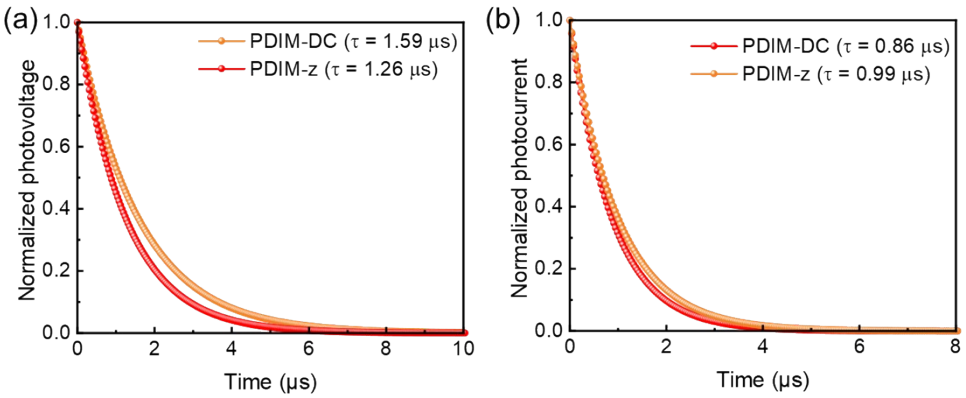

Figure S10. (a) TPV and (b) TPC decay traces of PDIM-DC and PDIM-z-based devices.

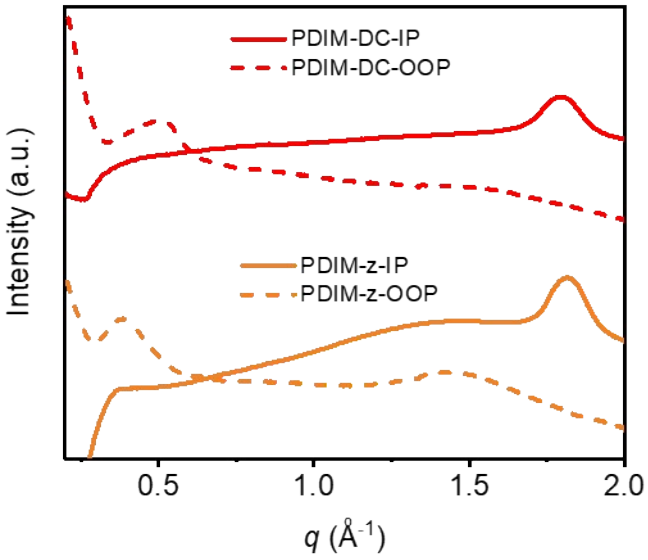

Figure 11. The corresponding linecut profiles of the 2D GIWAXS diffraction patterns of PDIM-DC and PDIM-z along the in-plane (IP, solid lines) and out-of-plane (OOP, dash lines) directions.

Table S7. Summary of *d*-spacing and crystalline coherence lengths for PDITh-SB, PDITh-PC, and PDITz-PC.

ETLs	π–π stacking			
	q (Å^{-1})	*d*-spacing[a] (Å)	FWHM (Å^{-1})	CCL[b] (Å)
PDIM-DC	1.781	3.53	0.106	52.76
	1.825	3.44	0.077	72.62
PDIM-z	1.815	3.46	0.104	53.77
	1.554	4.04	1.995	2.80

[a]The *d*-spacing values are calculated based on the equation $d = 2\pi/q$; [b]The coherence length (CCL) is derived from the Scherrer equation: $CCL = 2\pi K/\Delta q$, where K is the shape factor (typically 0.89) and Δq is the full width at half maximum (FWHM) of the diffraction peak.

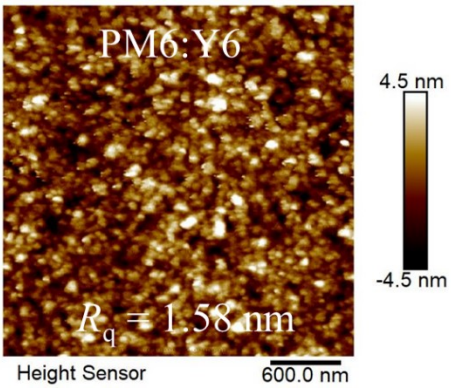

Figure S12. AFM height image of PM6:Y6 as the active layer.

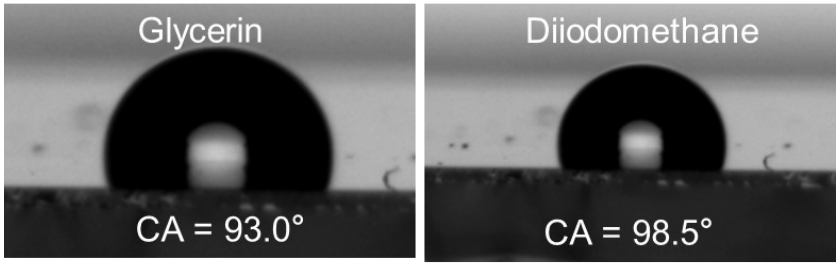

Figure S13. Contact angles of glycerol and diiodomethane on the surface of PM6:Y6 films.

Table S8. The surface energies (γ_s) of all the samples and the interfacial energies (γ_{ae}) between the ETLs and the PM6:Y6 active layer.

Surface	Contact angle (°)		Surface energy[a] (γ_s)	Interfacial energy[b] (γ_{ae})
	Glycerol	Diiodomethane	(mN m^{-1})	(mN m^{-1})
PM6:Y6	93.0°	98.5°	19.72	/
PDIM-DC	58.0°	54.1°	40.57	8.54
PDIM-z	37.4°	53.2°	51.63	14.26

[a]Surface energy (γ_S) was calculated from the equation $\gamma_{LV}(1+\cos\theta) = \frac{4\gamma_S^D\gamma_L^D}{\gamma_S^D+\gamma_L^D} + \frac{4\gamma_S^P\gamma_L^P}{\gamma_S^P+\gamma_L^P}$, γ_S consists of dispersion force γ_S^D and polarity force γ_S^P, γ_{LV} is the surface energy of a liquid which is composed of by the dispersion force γ_L^D and the polarity force γ_L^P; [b]Interfacial energy (γ_{ae}) was calculated by the formula of $\gamma_{ae} = \gamma_a + \gamma_c - W_a$, $W_a = 2\left[\left(\gamma_a^D \cdot \gamma_c^D\right)^{0.5} + \left(\gamma_a^P \cdot \gamma_c^P\right)^{0.5}\right]$, γ_a and γ_c are the surface energies of the active layer and the ETLs, respectively.

Table S9. Optimal performances of PM6:BTP-eC9-based devices with PDIM-DC and PDIM-z as the ETLs.

ETLs	V_{oc} [a] (V)	J_{sc} [a] (mA cm^{-2})	FF [a] (%)	PCE [a] (%)
PDIM-DC	0.853 (0.848±0.002)	27.98 [26.83[b]] (27.51±0.19)	78.02 (77.43±0.34)	18.61 (18.17±0.17)
PDIM-z	0.836 (0.830±0.002)	27.34 [26.68[b]] (27.27±0.20)	74.68 (72.80±0.92)	17.07 (16.66±0.30)

[a]Average value from at least 10 devices; [b]Calculated J_{sc} from EQE curves.

Table S10. Optimal performances of PM6:L8-BO-based devices with PDIM-DC and PDIM-z as the ETLs.

ETLs	V_{oc} [a] (V)	J_{sc} [a] (mA cm^{-2})	FF [a] (%)	PCE [a] (%)
PDIM-DC	0.913 (0.901±0.005)	25.79 [24.81[b]] (25.67±0.20)	78.01 (77.42±0.41)	18.38 (17.97±0.15)
PDIM-z	0.878 (0.871±0.004)	25.31 [24.52[b]] (25.11±0.21)	74.13 (72.77±0.58)	16.47 (16.23±0.14)

[a]Average value from at least 10 devices; [b]Calculated J_{sc} from EQE curve.

Table S11. Optimal performances of D18:L8-BO-based devices with PDIM-DC and PDIM-z as the ETLs.

ETLs	V_{oc} [a] (V)	J_{sc} [a] (mA cm^{-2})	FF [a] (%)	PCE [a] (%)
PDIM-DC	0.925 (0.919±0.007)	26.26 [25.03[b]] (26.13±0.14)	79.02 (78.90±0.34)	19.19 (18.96±0.05)
PDIM-z	0.882 (0.876±0.004)	26.16 [24.88[b]] (26.09±0.15)	75.78 (75.01±0.56)	17.48 (17.13±0.18)

[a]Average value from at least 10 devices; [b]Calculated J_{sc} from EQE curve.

5. NMR spectra

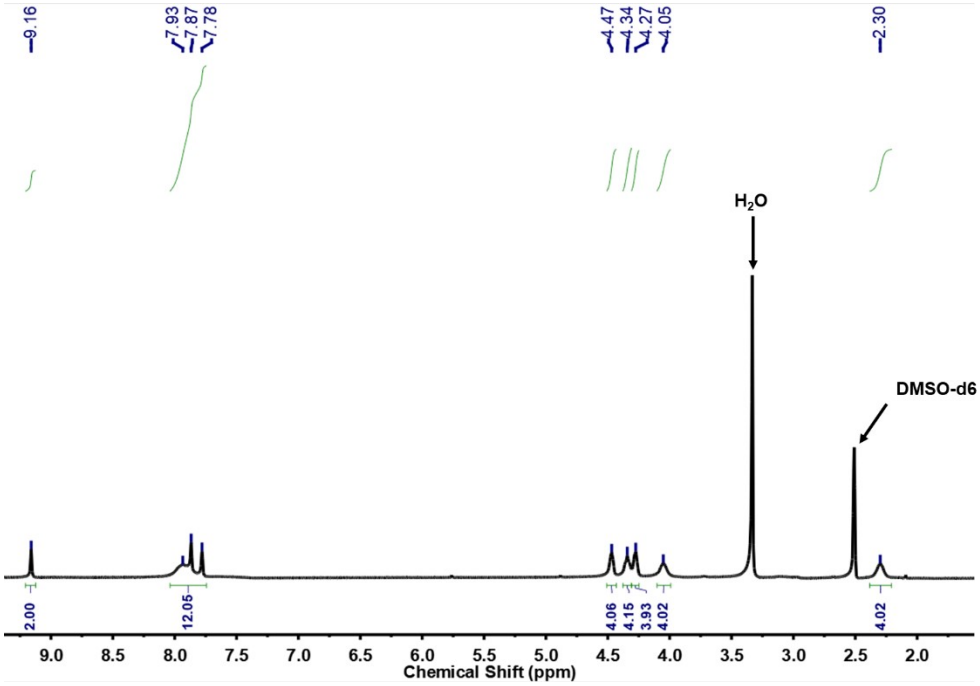

Figure S14. ^{1}H NMR of PDIM-DC (400 MHz, DMSO-d_6).

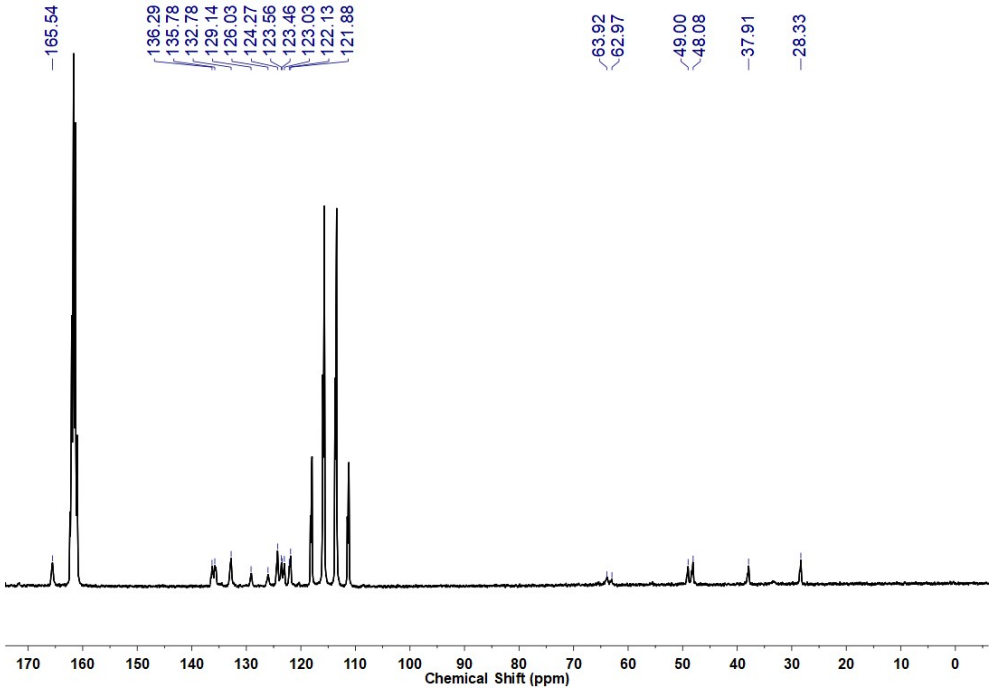

Figure S15. ^{13}C NMR of PDIM-DC (101 MHz, TFA-*d*).

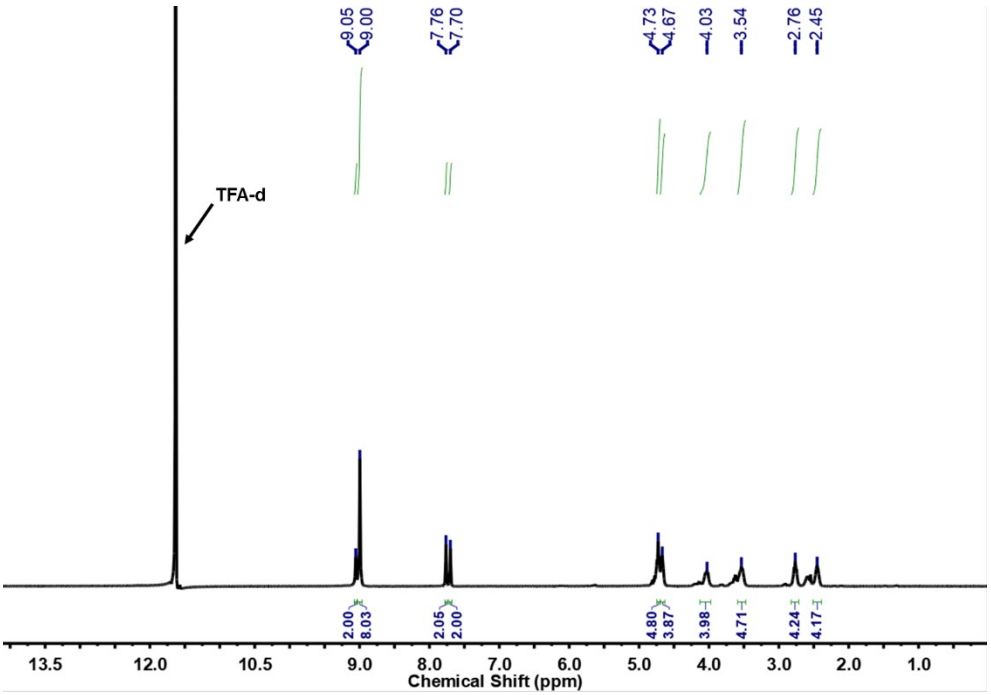

Figure S16. ^{1}H NMR of PDIM-z (400 MHz, TFA-*d*).

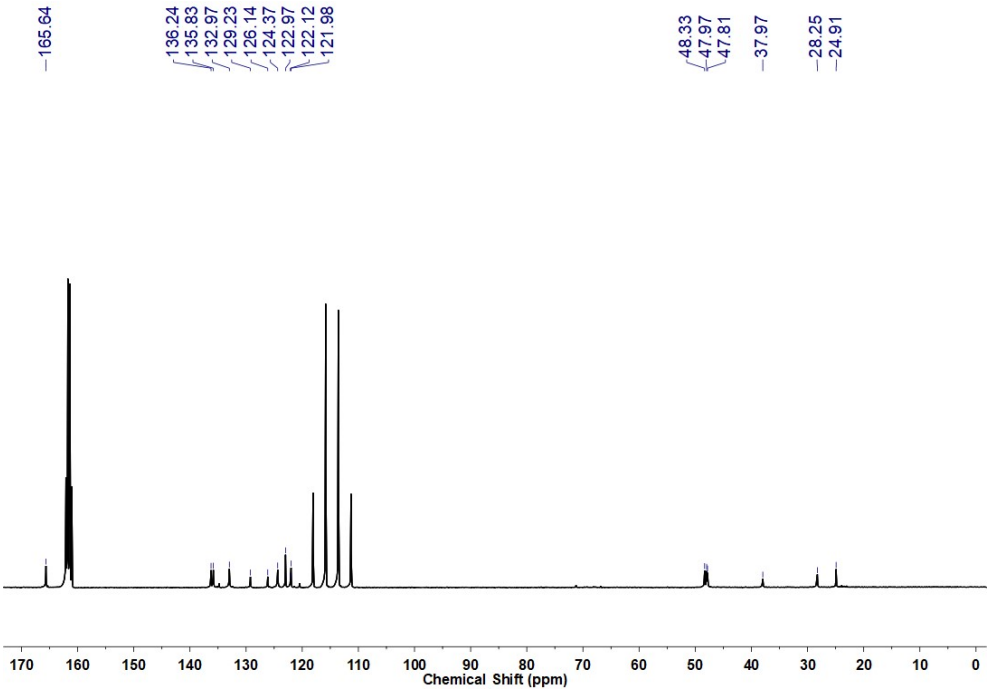

Figure S17. ^{13}C NMR of PDIM-z (101 MHz, TFA-*d*).

6. Reference

1. M. Liu, Y. Jiang, D. Liu, J. Wang, Z. Ren, T. P. Russell and Y. Liu, *ACS Energy Lett.*, **2021**, *6*, 3228-3235.

2. G. Li, X. Mo, J. Zhou, Z. Xia, D. Jiang, P. Ren, H. Zhao, R. Wang, Z. Liu and S. Pu, *Dyes Pigm.*, **2026**, 247, 113491.

3. D. K. Owens and R. C. Wendt, *J Appl. Poly. Sci.*, **2003**, 13, 1741-1747.